Supporting Information

Design of Coherent Anode Materials with 0D Ni_3S_2 Nanoparticles Self-assembled on 3D Interconnected Carbon Networks for Fast and Reversible Sodium Storage

Xu Zhao, [a, b, c] Hong-En Wang, [c] Robert C. Massé, [c] Jian Cao, [a] Jiehe Sui, [a,b] Jiangyu Li, [d] Wei Cai, [b]* and Guozhong Cao [c]*

[a] State Key Laboratory of Advanced Welding and Joining, Harbin Institute of Technology, Harbin 150001, China.

[b] School of Materials Science and Engineering, Harbin Institute of Technology, Harbin 150001, China.

[c] Department of Materials Science and Engineering, University of Washington, Seattle, WA 98195, USA.

[d] Department of Mechanical Engineering, University of Washington, Seattle, WA 98195, USA.

Corresponding author: weicai@hit.edu.cn; gzcao@u.washington.edu

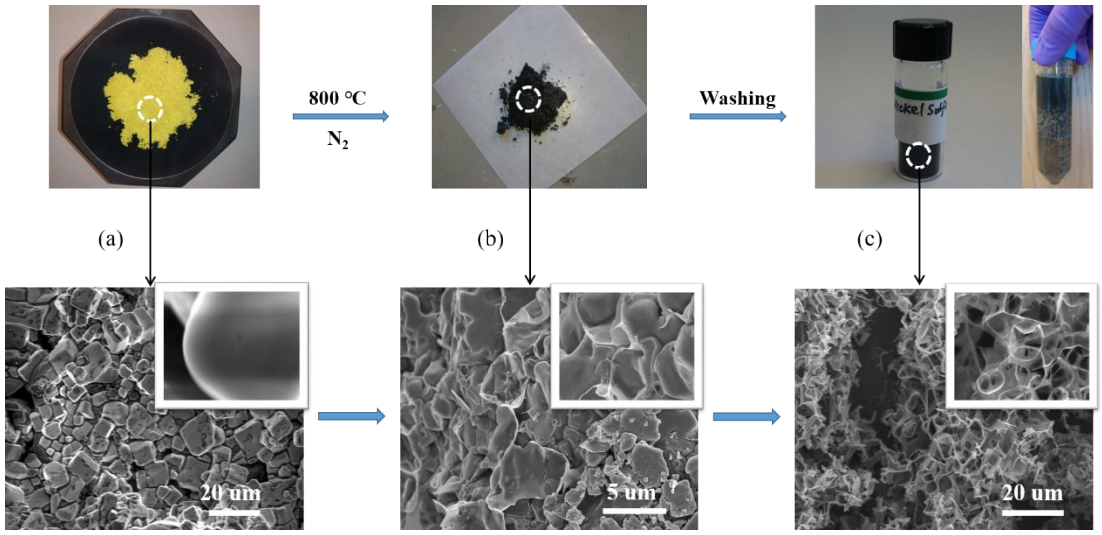

Figure S1. Optical photograph and corresponding SEM images of different periods in preparing coherent Ni_3S_2/C nanocomposites: (a) $Ni(NO_3)_2 \cdot 6H_2O$ + citric acid + thiourea adsorbed NaCl after freeze-drying, SEM demonstrating a uniform attaching of $Ni(NO_3)_2 \cdot 6H_2O$ + citric acid + thiourea precursors onto NaCl cubic surface; (b) Ni_3S_2/C adsorbed NaCl after annealing in N_2 (800 ^{0}C in N_2 for 2h, ramping rate was 5 ^{0}C/min), SEM indicating as-prepared Ni_3S_2/C coated on the cubic surface of NaCl template homogeneously; (c) coherent Ni_3S_2/C hybrids after NaCl removal, which has a low density to float on water, SEM images show an overall porous interconnected nanostructure.

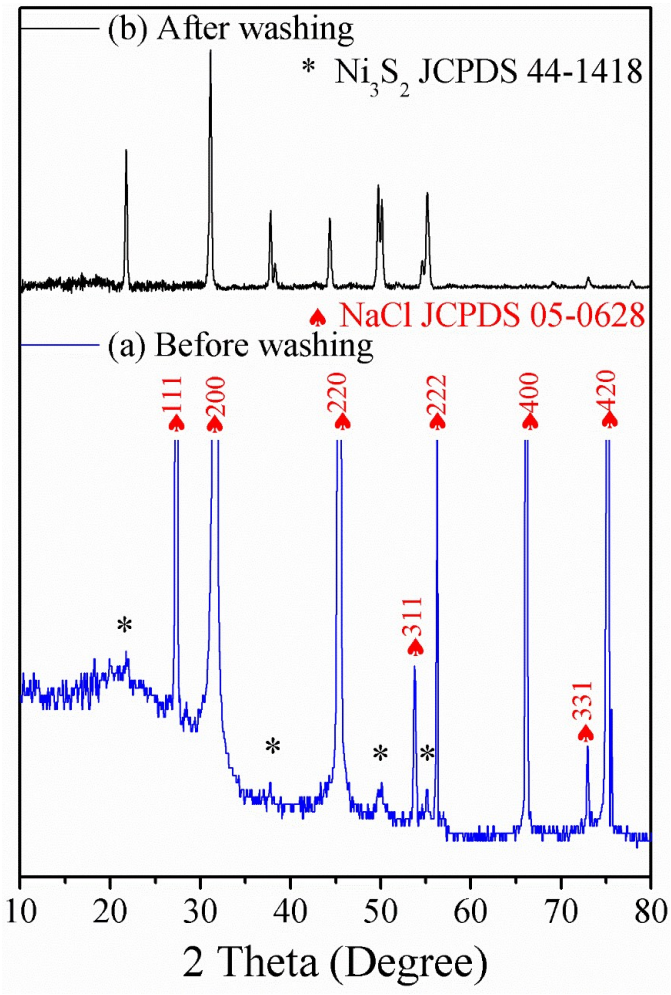

Figure S2. XRD patterns of coherent Ni_3S_2/C nanocomposite (a) before and (b) after washing to dissolve NaCl templates, in addition to strong peaks of cubic phase NaCl (*JCPDS No. 87-0712*), other peaks are in good accordance with Ni_3S_2 of Heazlewoodite phase (*JSPDS No. 44-1418*).

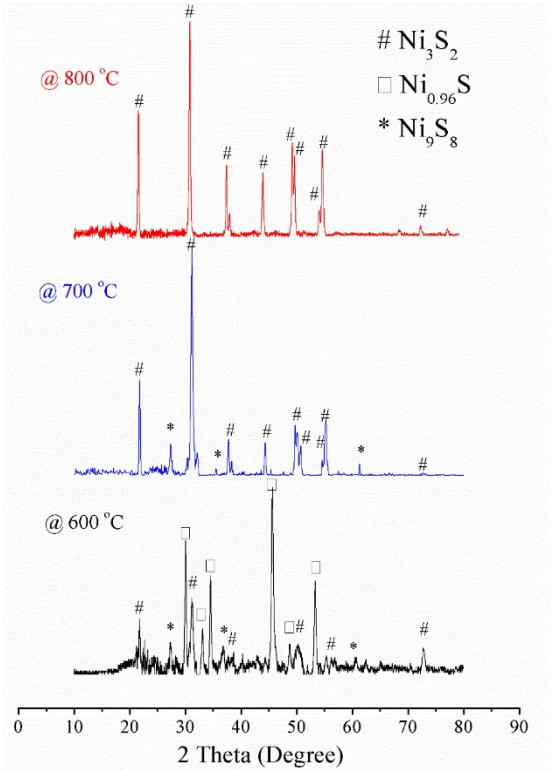

Figure S3. Influence of annealing temperatures (600 ^{0}C, 700 ^{0}C and 800 ^{0}C in N_2 for 2h, ramping rate: 5 ^{0}C/min) on phase purity of coherent Ni_3S_2/C nanocomposite. Results indicate Ni_3S_2 can be a more stable phase in nickel sulfides and high temperature is helpful to form phase-purity Ni_3S_2/C.

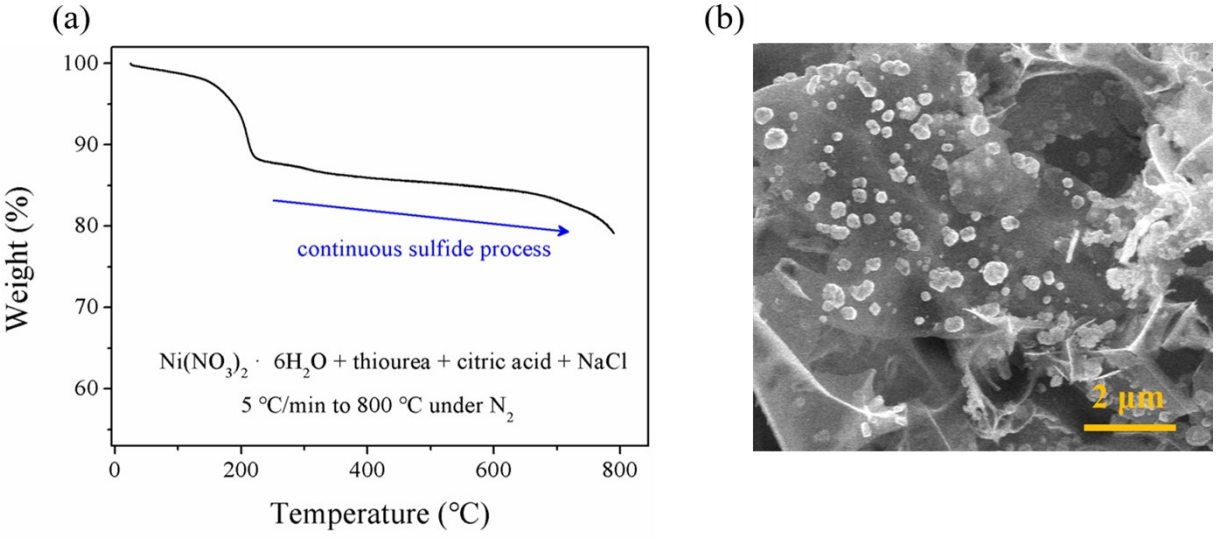

Figure S4. (a) TGA result of "$Ni(NO_3)_2$ + thiourea + citric acid + NaCl" composites at temperatures ranging from room temperature to 800 ^{0}C in N_2 with a heating rate of 5 ^{0}C/min; (b) SEM image of of Ni_3S_2/C synthesized by l-cysteine

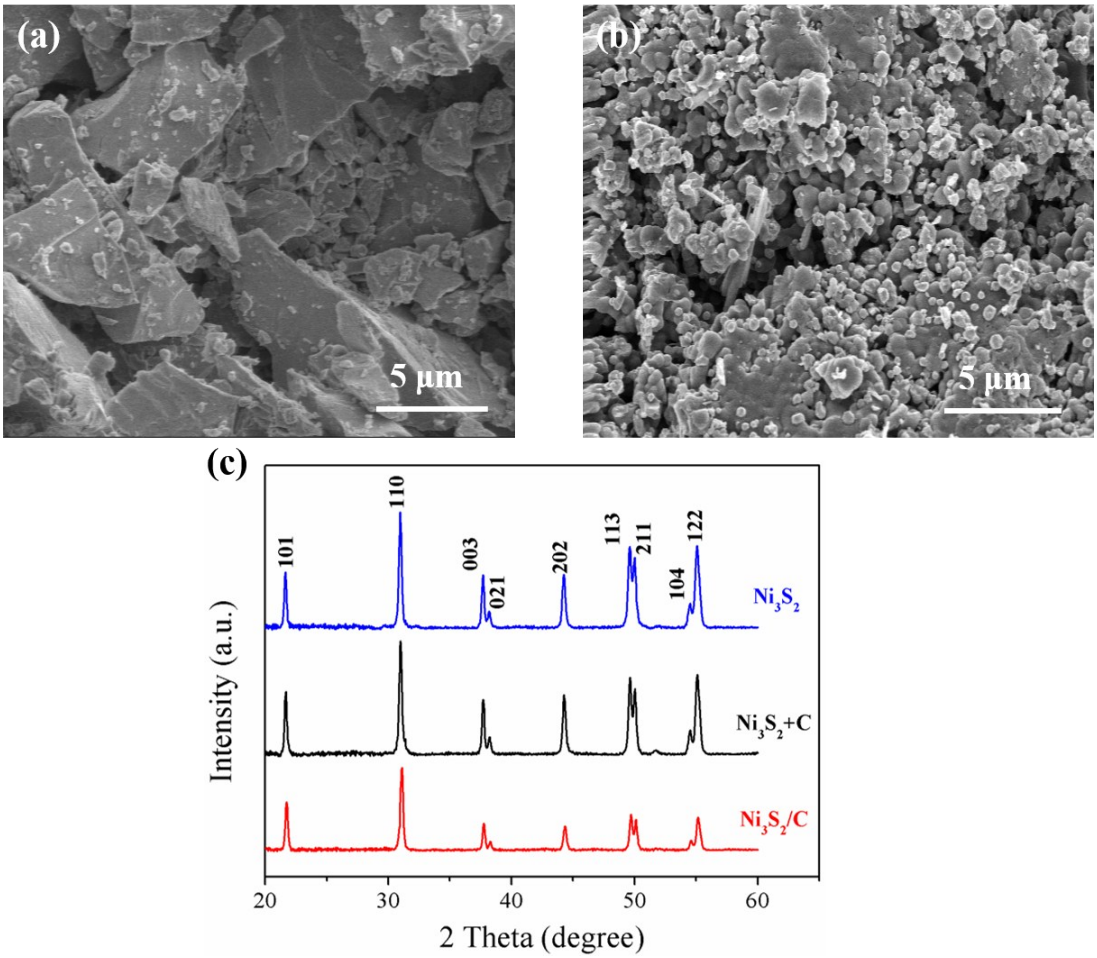

Figure S5. Low magnification SEM images of (a) bare Ni_3S_2 without adding the carbon precursor, confirming the carbon can provide abundant surfaces for reactions and prevent Ni_3S_2 nanoparticles from agglomeration during the annealing process; (b) bulk Ni_3S_2+C without adding NaCl templates, showing a key role of NaCl templates plays an indispensable role in the formation of homogeneous coherent nanostructures; (c) XRD results of bare Ni_3S_2, bulk Ni_3S_2+C and coherent Ni_3S_2/C, indicating that phase purity of as-prepared samples.

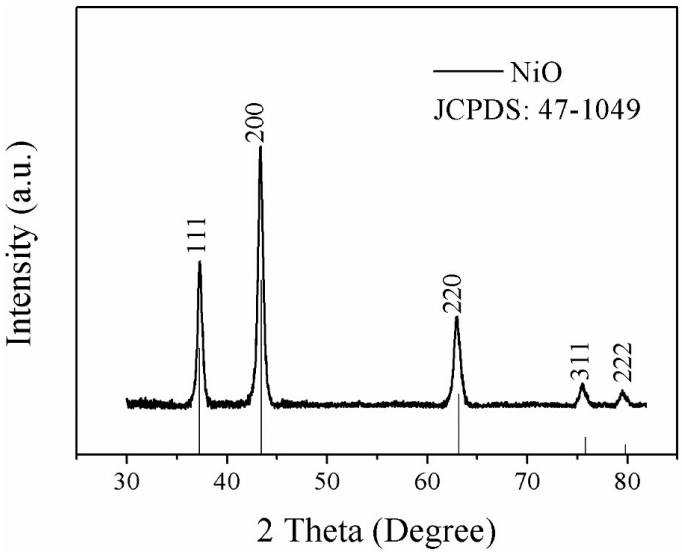

Figure S6. XRD pattern of coherent Ni_3S_2/C nanocomposite after TGA measurement in air (20 ^{0}C to 700 ^{0}C, ramping rate: 10 ^{0}C/min), indicating Ni_3S_2 transfer completely into NiO (*JCPDS No. 47-1049*).

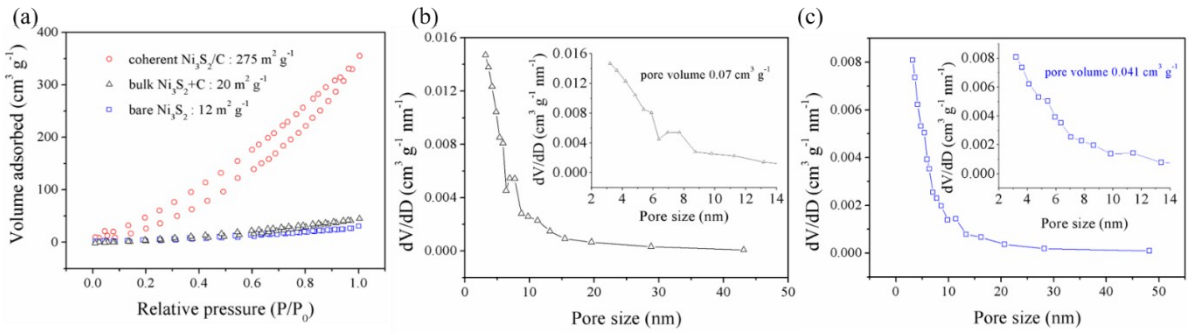

Figure S7. (a) Nitrogen sorption isotherms of coherent Ni_3S_2/C composites, bulk Ni_3S_2+C and bare Ni_3S_2, the BET surface areas were determined by a *multi-point-BET* method; Pore size distribution of (b) bulk Ni_3S_2+C and (c) bare Ni_3S_2, the pore volumes were determined by *BJH-Desorption* method.

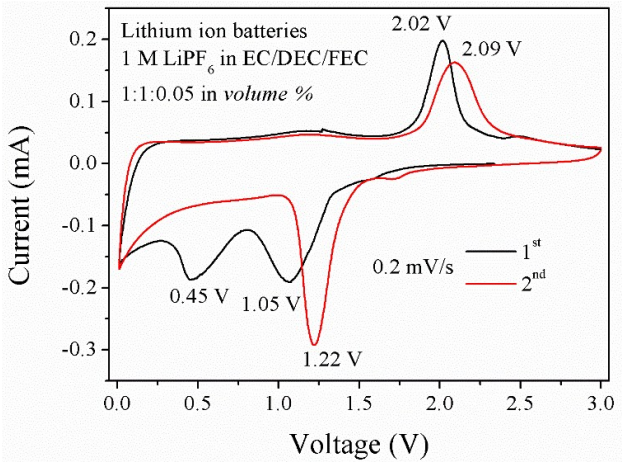

Figure S8. CV curves of coherent Ni_3S_2/C in lithium ion batteries under a scan rate of 0.2 mV/s. Electrolyte was 1 M $LiPF_6$ in EC/DEC/FEC, 1:1:0.05 in volume %.

In the first scan, two cathodic peaks at 1.05 V and 0.45 V and one anodic peak at 2.02 V can be clearly distinguished. The peak located at 1.05 V can be ascribed to the insertion of lithium ion into Ni_3S_2. The broad peak at about 0.45 V might be the conversion reaction as well as the formation of SEI and decomposition of electrolyte, which corresponded well with that of SIBs. After activating in the first cycle, one couple at 1.22 V / 2.09 V could be recognized. Total electrochemical reaction can be described in Equation (1). The potential is similar to that of sodium ion batteries.

$$Ni_3S_2 + 4\ Li^+ + 4\ e^- \leftrightarrow 3\ Ni + 2\ Li_2S \qquad (1)$$

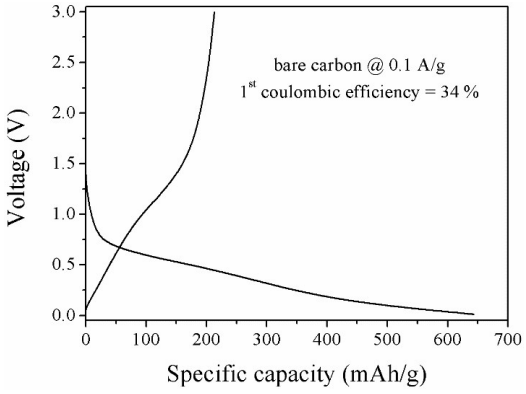

Figure S9. Discharge/charge curves of bare carbon networks under 0.1 A/g in 0 ~ 3 V, which shows a low coulombic efficiency of 34 %.

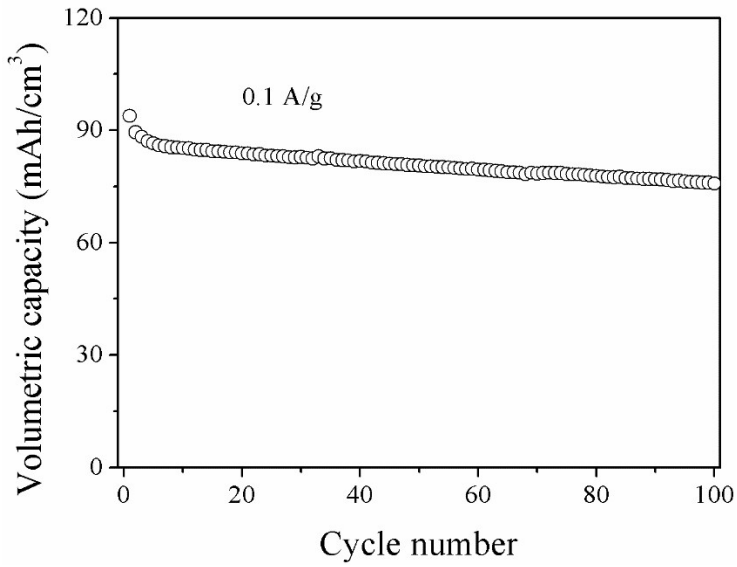

Figure S10. Volumetric capacity of coherent Ni_3S_2/C electrode under 0.1 A/g. The calculation is based on whole anode coating volume.

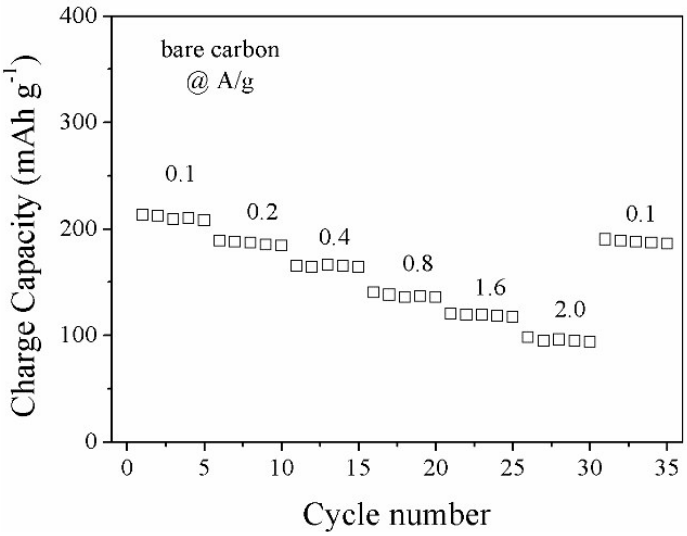

Figure S11. Rate performances of pure carbon matrix.

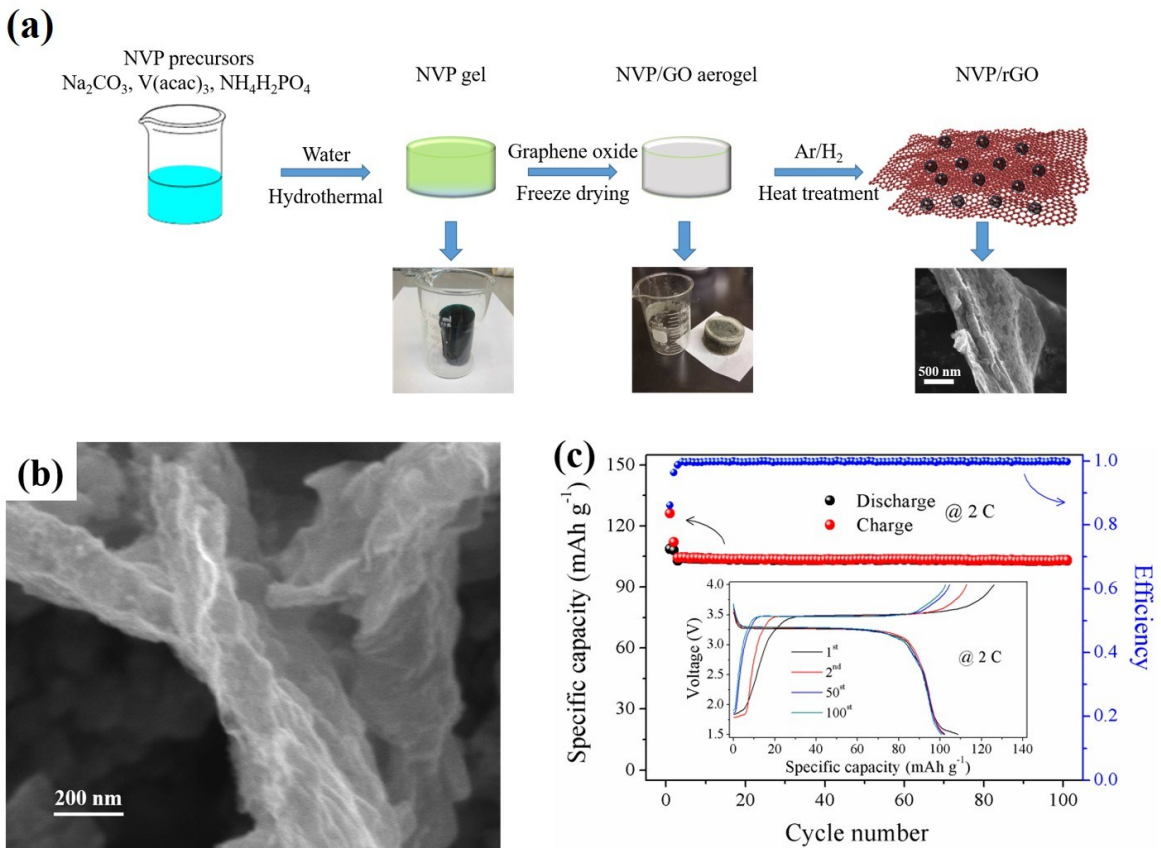

Figure S12. (a) Schematic Illustration and optical photograph in different steps of preparing $Na_3V_2(PO_4)_3$/rGO *via* sol-gel and post-annealing methods; (b) SEM of $Na_3V_2(PO_4)_3$/rGO lamellar structure with multi-stacked structures, (c) Cyclic performance and efficiencies of $Na_3V_2(PO_4)_3$/rGO at 2 C for 100 cycles (1 C≈ 110 mA g^{-1}; the inset is the charge/discharge curves at 1st, 2nd, 5st and 100st cycles, flat charge and discharge plateaus at around 3.3 and 3.5 V, corresponding to the redox pair of V^{3+}/V^{4+}).

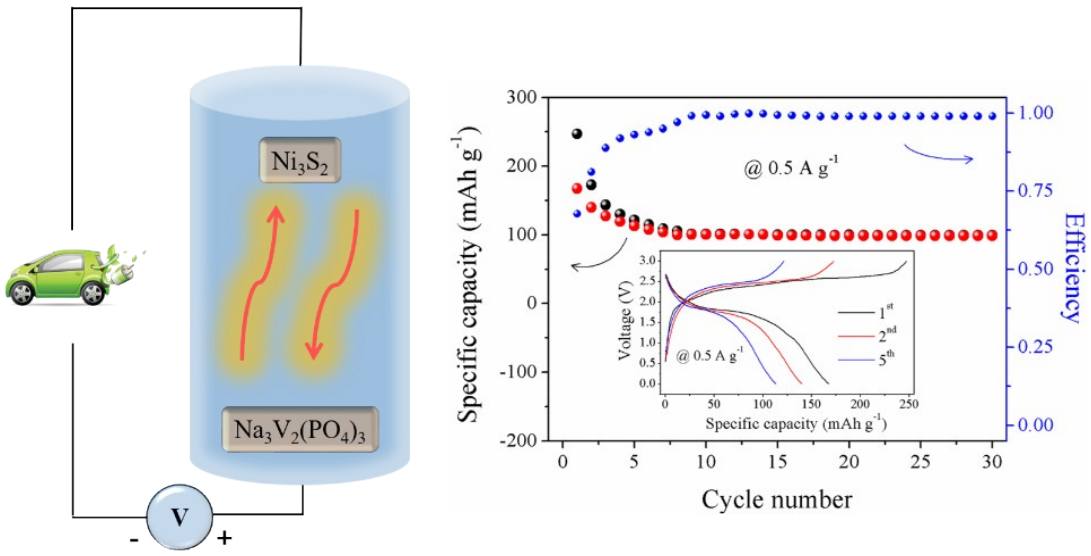

Figure S13. Illustration of the composition and cycling performance of $Na_3V_2(PO_4)_3$/rGO cathode || Ni_3S_2/C anode full cell at 0.5 A g^{-1} (the inset is the charge/discharge curves at 1st, 2nd, 5th cycles, The open potential of fresh full-cell is about 0.5 V, which may be caused by the high internal resistance; mass ratio between cathode and anode was 6:1).

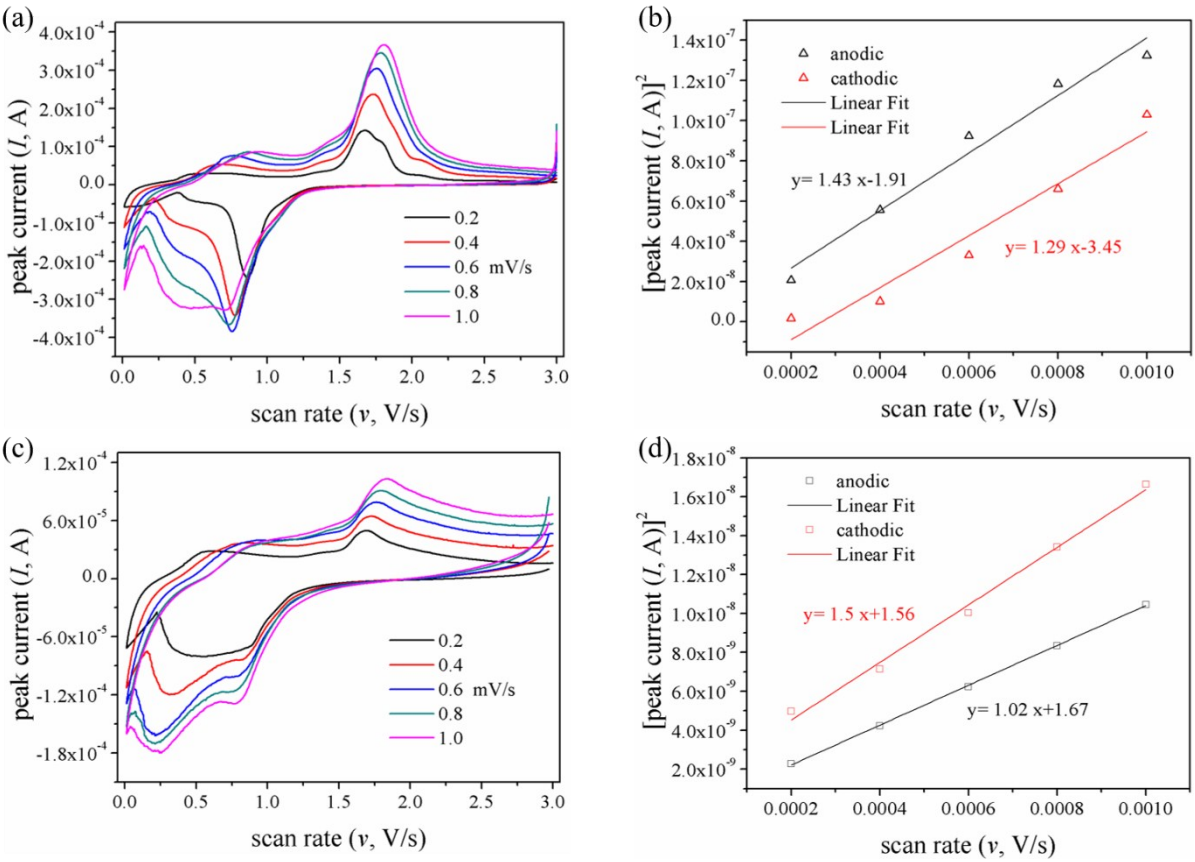

Figure S14. Cyclic voltammetry curves of (a) the bulk Ni_3S_2+C electrode and (c) bare Ni_3S_2 electrode at different scan rates; I^2 as a function of v for (b) bulk Ni_3S_2+C electrode and (d) bare Ni_3S_2 electrode. For bulk Ni_3S_2+C electrode, the D is 5×10^{-13} and 4.5×10^{-13} cm^2 g^{-1} for anodic peak and cathodic peak, respectively. For bare Ni_3S_2 electrode, the D is 3.6×10^{-13} and 5.2×10^{-13} cm^2 g^{-1} for anodic peak and cathodic peak, respectively.

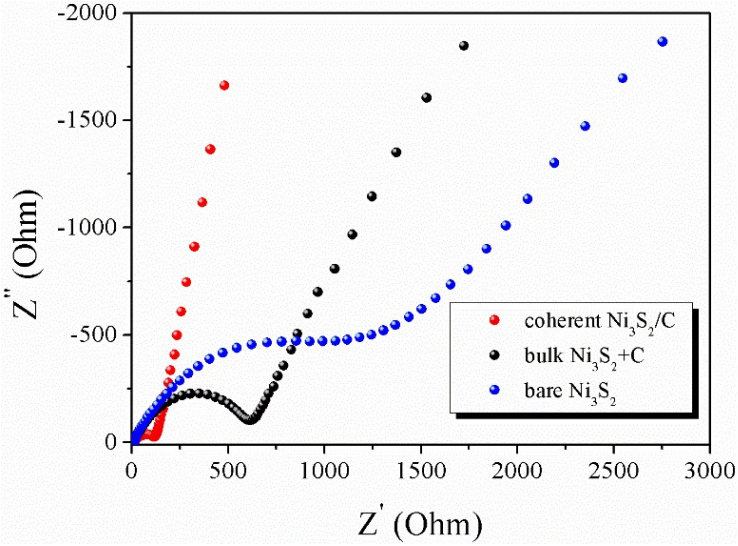

Figure S15. Nyquist plots of coherent Ni_3S_2/C composites, bulk Ni_3S_2+C and bare Ni_3S_2 after 135 cycles under various rates, the coherent structure has lowest charge-transfer resistance and fastest sodium ion diffusion among listed three samples.

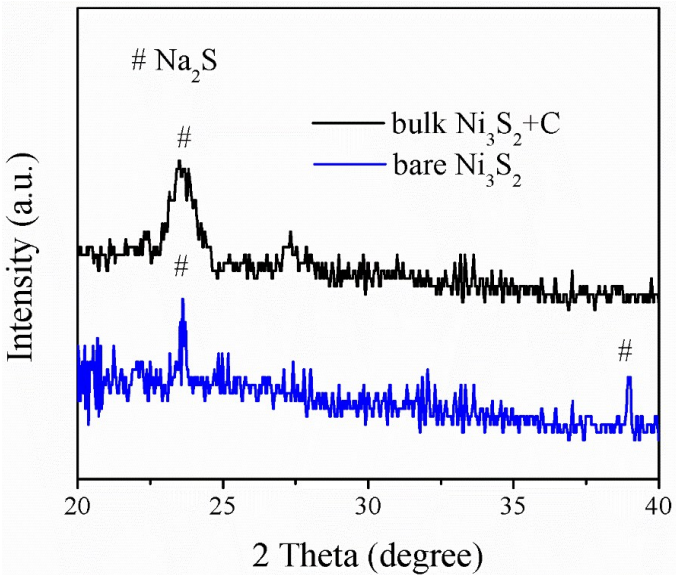

Figure S16. XRD patterns of electrodes at charge state (3.0 V) for bulk Ni_3S_2+C and bare Ni_3S_2. Results indicate the irreversible reactions of bulk Ni_3S_2+C and bare Ni_3S_2 after first cycle, demonstrating the key role of coherent structure to reversible reactions.

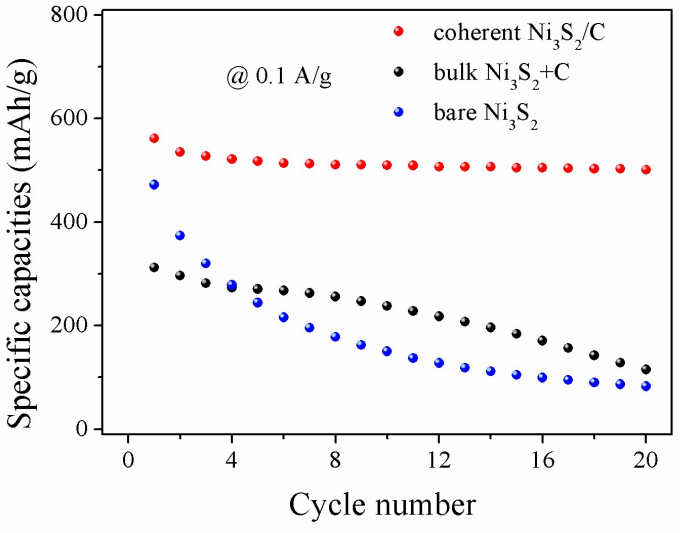

Figure S17. Cyclic performances of coherent Ni_3S_2/C, bulk Ni_3S_2 + C and bare Ni_3S_2 under a low current density of 0.1 A/g.

Table S1. Comparison of specific capacity and capacity retention at different current densities for Ni_3S_2 composite electrode with other Ni_3S_2 based anodes in SIBs.

Materials	Voltage range (V)	Current density (A/g)	Cycle number	Specific capacity after cycle (mAh/g)	Capacity retention (%)
Coherent Ni_3S_2/C networks (This work)	**0.01~3.0**	**0.1**	**100**	**453**	**85**
		0.4	**100**	**430**	**87**
		2.0	**200**	**409**	**96**
PEDOT@Ni_3S_2 on Ni foam [ref 30]	0.5~2.8	0.6	50		50
Nickel sulfide nanoparticles with an ultrathin carbon layer [ref 31]	0.01~3.0	0.1	200	340	85
Layered nickel sulfide-reduced graphene oxide [ref 32]	0.005~3.0	0.1	50	392	76
Different morphologies of Ni_3S_2 on Ni foam [ref 33]	0.01~3.0	0.05	100	315	85